

# Optimization design of microchannel heat sink geometry for high power laser mirror

Haishan Cao<sup>a,b</sup>, Guangwen Chen<sup>a,\*</sup>

<sup>a</sup>Dalian Institute of Chemical Physics, Chinese Academy of Sciences, Dalian 116023, China

<sup>b</sup>Graduate University, Chinese Academy of Sciences, Beijing 100049, China

## ARTICLE INFO

### Article history:

Received 31 May 2009

Accepted 18 March 2010

Available online 25 March 2010

### Keywords:

Microchannel

Heat sink

Laser mirror

Heat transfer

## ABSTRACT

Microchannel heat sink for high power laser mirror with water cooling was analyzed as a function of microchannel geometry and operation parameters. A comparative analysis of the thermal deformation on the mirror surface without cooling and that with cooling revealed that the maximal thermal deformation on the mirror surface could decrease from about 0.115  $\mu\text{m}$  to around 0.040  $\mu\text{m}$  under the laser power of 200  $\text{W}/\text{cm}^2$  by using microchannel heat sink designed. In order to enhance the performance of microchannel heat sink, the effects of channel width, channel depth, fin width, mirror thickness and cooling region were investigated. The results indicated that the heat transfer performance of the microchannel heat sink could be further improved by narrow and deep channel, narrow fin, thin mirror and large cooling region.

© 2010 Elsevier Ltd. All rights reserved.

## 1. Introduction

The heat-induced deformation of laser mirror has become a serious obstacle to the development of high power laser with the increase of laser power and working time. When the thermal deformation exceeds a critical value, the beam quality will decline prominently; and in the worse situation the mirror will destruct, or even burst. More accurately, if the amount of deformation is from  $L/10$  to  $L/4$ , the laser beam quality will decline sharply and the laser output power will decrease obviously [1]. Therefore, it is crucial to keep the mirror temperature within a certain range. In order to resolve the problem, many researchers have presented different ways to prevent the deformation of mirror by reducing thermal effect [2–5].

Kasamatsu et al. [2] presented the constitution of a cooling type total reflecting mirror that the cooling water, as coolant through the rear surface of a reflecting mirror, was recycled so as to cool the reflecting mirror and the outside frame. Bluege [3] reported a phase change cooling technique for mirror including a mirror substrate with a reflective front major surface and a rear major surface. Rosenfeld and North [4] introduced heat exchangers based on porous media which could be used to cool high heat load optical components as well as other high heat flux applications. Lee and Kim [5] analyzed the performance of the thermoelectric cooler and concluded that increasing the element thickness with the large

number of thermoelectric pairs or decreasing the cross sectional area of the element can improve the performance.

Compared with the liquid cooling, the phase change cooling and the thermoelectric cooling can avoid the vibration and distortion of the mirror. However, the cooling effect of the phase change cooling is limited by the time interval between two shoots in the high power laser. Furthermore, the thermoelectric cooling efficiency is limited by the figure of merit [6,7].

In this study, the cooling technology using microchannel heat sink with special geometrical configuration was designed to minimize the thermal deformation and weaken the vibration and distortion, which were induced by temperature rise and water impact. The present work was inspired by a technique designed by Tuckerman and Pease [8], in which microchannels ( $50 \times 300 \mu\text{m}$ ) were etched in a  $\langle 100 \rangle$  silicon wafer of 400  $\mu\text{m}$  thickness. The authors observed that the heat transfer coefficient increased with decreasing channel width for laminar flow in a channel. Subject to the designed dimensions, a heat flux of 790  $\text{W}/\text{cm}^2$  was achieved with a maximum substrate temperature rise of 71 K using water as the coolant.

The Nusselt number is an important parameter for the optimum design of microchannel heat sink. Nevertheless, whether the Nusselt number in microchannels agrees with conventional classical theory in both the laminar and turbulent regimes still remains as one of the most controversial issues.

Shortly after the initial work of Tuckerman and Pease, Wu and Little [9] conducted experiments to measure heat transfer characteristic of nitrogen gas in the trapezoidal silicon microchannels

\* Corresponding author. Tel.: +86 411 84379031; fax: +86 411 84379327.  
E-mail address: [gwchen@dicp.ac.cn](mailto:gwchen@dicp.ac.cn) (G. Chen).

**Nomenclature**

$a$	channel width, mm
$A$	total heat exchanger area of microchannel heat sink, mm <sup>2</sup>
$A_c$	cross sectional area of fin, mm <sup>2</sup>
$b$	channel depth, mm
$c$	fin width, mm
$c_p$	specific heat, J/kg K
$d$	mirror thickness, mm
$d_h$	hydraulic diameter, mm
$E$	young modulus, GPa
$G$	shear modulus, GPa
$h$	heat transfer coefficient, W/m <sup>2</sup> K
$h_e$	effective heat transfer coefficient, W/m <sup>2</sup> K
$I(r,t)$	laser power density, W/cm <sup>2</sup>
$k$	thermal conductivity of mirror, W/m K
$k_c$	thermal conductivity of coolant, W/m K
$k_f$	thermal conductivity of fin, W/m K
$l_i$	length of each channel, mm
$L$	laser wavelength, nm
$m$	fin efficiency constant defined by Eq. (11)
$n$	number of channels
$Nu$	Nusselt number
$P$	perimeter of microchannel, mm
$Q$	volumetric flow rate, mL/min
$r$	radial coordinate
$r_0$	irradiation region radius, mm
$r_1$	cooling region radius, mm

$r_2$	mirror radius, mm
$Re$	Reynolds number
$T$	temperature of mirror, K
$T_0$	ambient temperature, K
$T_c$	temperature of cooling water, K
$u$	velocity of fluid through each microchannel, m/s
$u_r$	displacement in $r$ direction, $\mu\text{m}$
$u_z$	displacement in $z$ direction, $\mu\text{m}$
$z$	longitudinal coordinate

**Greek symbols**

$\alpha$	channel aspect ratio defined by Eqs. (7) and (9)
$\alpha_T$	thermal expansion coefficient, K <sup>-1</sup>
$\gamma_{rz}$	shear strain in the $rz$ direction
$\varepsilon$	volume strain
$\varepsilon_r$	normal strain in $r$ direction
$\varepsilon_z$	normal strain in $z$ direction
$\varepsilon_\theta$	normal strain in $\theta$ direction
$\nu$	Poisson's ratio
$\rho$	density, kg/m <sup>3</sup>
$\sigma_r$	normal stress in $r$ direction, Pa
$\sigma_z$	normal stress in $z$ direction, Pa
$\sigma_\theta$	normal stress in $\theta$ direction, Pa
$\eta$	reflectivity
$\eta_f$	fin efficiency
$\lambda$	Lame constant, GPa
$\theta$	azimuthal coordinate
$\mu$	kinematic viscosity, Pa s
$\tau_{rz}$	shear stress in the $r z$ direction, Pa

with widths of 312–574  $\mu\text{m}$  and depths of 89–97  $\mu\text{m}$ , and found average Nusselt numbers were higher than those predicted by the conventional correlations for fully-developed laminar and turbulent flows. The authors considered the very large relative roughness of microchannels could improve heat transfer coefficient.

Rahman and Gui [10] found the Nusselt number was high in the laminar regime and low in the turbulent regime through the experiment on heat transfer characteristics of water in microchannels etched in <100> silicon wafers. Wang and Peng [11] investigated the forced convection of water and methanol in stainless steel rectangular microchannels. The result showed that the liquid velocity, liquid properties and geometry of microchannels all had significant influences on the heat transfer coefficient. However, Wang and Peng have not compared their results with the conventional correlation. Harms et al. [12] concluded the local Nusselt number agreed reasonably well with classical developing channel flow theory via the test of the single-phase developing convection of water in <110>silicon rectangular microchannels.

Qu and Mudawar [13] investigated the heat transfer characteristics of a single-phase microchannel heat sink consisted of an array of rectangular microchannels with width of 231  $\mu\text{m}$  and depth of 713  $\mu\text{m}$ , which was fabricated by using oxygen-free copper as the base and a polycarbonate plastic plate as the cover. The results showed that the conventional Navier–Stokes and energy equations can adequately predict the fluid flow and heat transfer characteristics of microchannel heat sinks. Lin and Yang [14] tested forced convection heat transfer performance of water in two stainless steel tubes with inside diameter of 123  $\mu\text{m}$  and 962  $\mu\text{m}$  by means of a non-contacted liquid crystal thermography (LCT) method for micro tube surface temperature measurement. The test results fitted very well with those ones predicted by the conventional correlations.

From a chronological analysis of the experiment results, the deviations between the heat transfer behavior in microchannels and the one in large-sized channels are decreasing, due to the rapid improvement of micro fabrication and advanced measurement means. Nowadays, most researchers tend to support the viewpoint that the conventional theory on the Nusselt number is still to be valid for microchannels.

In this study, the analysis is based on the correlation of Nusselt number for fully-developed laminar flow quoted Shah and London [15] and introduced by Philips [16], who has detailedly analyzed the forced convection and liquid cooled microchannel heat sinks.

**2. Analysis**

The structure of microchannel heat sink operating with water used to cool down the high power laser mirror and the cross section of microchannels are shown in Fig. 1. The effects of the inlet and outlet chambers are designed to weaken the direct impact of cooling water to the mirror and to eliminate the vibration and distortion of the mirror as far as possible. The number of microchannels that can be accommodated in given  $a$ ,  $c$  and  $r_1$  (radius of water cooling region) is given by

$$na + (n - 1)c = 2r_1 \quad (1)$$

The length of each channel  $l_i$  ( $1 \leq i \leq n$ ) is fixed by its position in given  $a$ ,  $c$  and  $r_1$ , as shown in Fig. 1.

The hydraulic diameter  $d_h$  is calculated from the microchannel dimensions as

$$d_h = \frac{4ab}{2(a+b)} \quad (2)$$

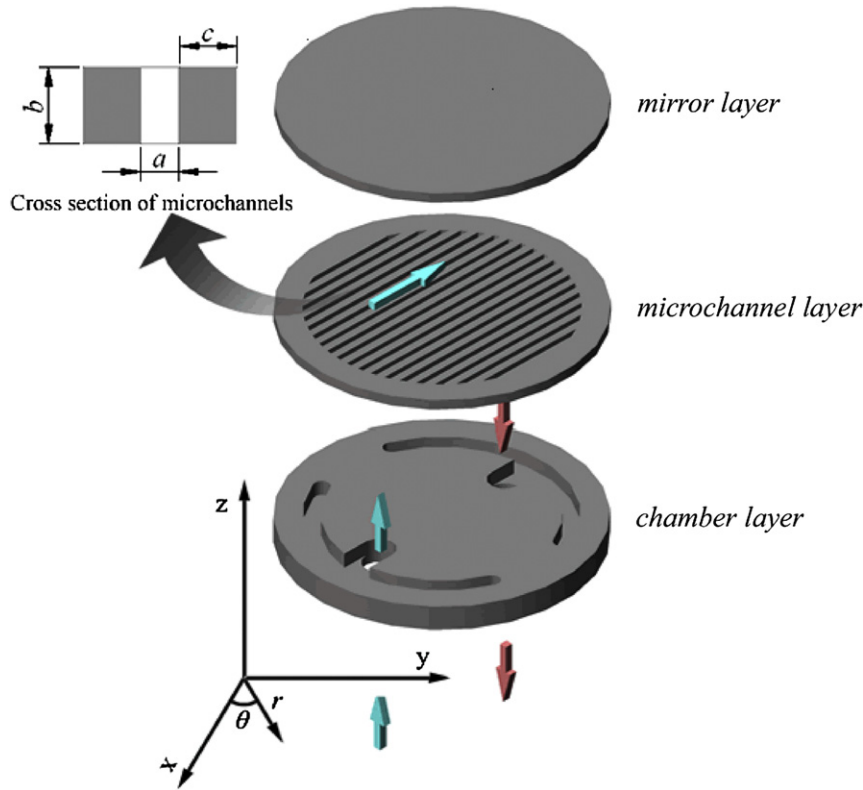


Fig. 1. Decompose diagram of the microchannel heat sink.

The velocity of fluid,  $u$ , through each microchannel, is calculated via

$$u = \frac{Q}{nab} \quad (3)$$

where  $Q$  is the total volumetric flow rate.

The Reynolds number for each microchannel is

$$Re = \frac{d_h u \rho}{\mu} \quad (4)$$

To determine the thermal performance of microchannel heat sink, it is necessary to know the value of the heat transfer coefficient, which is given by

$$h = \frac{Nu \cdot k_c}{d_h} \quad (5)$$

The Nusselt number is a function of several parameters, some of which are: the microchannel geometry, the coolant properties, the coolant flow rate and the flow regime (laminar, transitional, or turbulent).

In channel flow, the Nusselt number at the channel entrance is indefinitely high. In this study, it is assumed that the channel flow is fully-developed laminar flow. Thus the Nusselt number obtained in this way will be conservative. Fig. 2 shows the Nusselt number for fully-developed flow in rectangular channels with three walls transferring heat under uniform axial heat flux and uniform peripheral wall temperature.

The equation of the Nusselt number with  $\alpha$  by the least square fitting is expressed as follows,

$$Nu = 8.2327(1 - 1.8826\alpha + 3.7671\alpha^2 - 5.8139\alpha^3 + 5.3607\alpha^4 - 1.9993\alpha^5) \quad (6)$$

where

$$\alpha = a/b (b \geq a) \quad (7)$$

$$Nu = 5.3836(1 - 2.6872\alpha + 6.7527\alpha^2 - 8.3468\alpha^3 + 5.0862\alpha^4 - 1.1444\alpha^5) \quad (8)$$

where

$$\alpha = b/a (b \leq a) \quad (9)$$

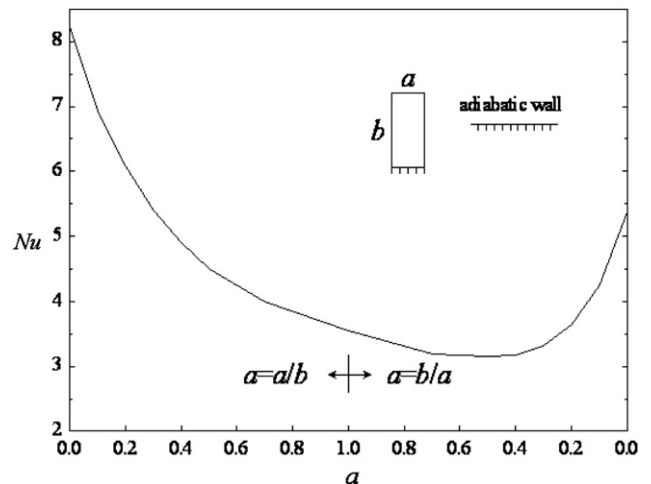


Fig. 2. The Nusselt number as a function of  $\alpha$  for a microchannel with three walls transferring heat.

The walls separating the microchannels can be treated as rectangular fins. The fin efficiency given by Eckert and Drake [17] is shown as follow,

$$\eta_f = \frac{\tan h(mb)}{mb} \quad (10)$$

where

$$m = \sqrt{\frac{hP}{k_f A_c}} \quad (11)$$

The total heat exchanger area  $A$  of microchannel heat sink is calculated as

$$A = \sum_{i=1}^{i=n} (al_i + 2bl_i\eta) \quad (12)$$

The simulation model is the mirror layer part in Fig. 1. The temperature distribution in laser mirror is given by the following heat conduction equation [18].

$$\rho c_p \frac{\partial T}{\partial t} - k \left[ \frac{1}{r} \times \frac{\partial}{\partial r} \left( r \frac{\partial T}{\partial r} \right) + \frac{\partial^2 T}{\partial z^2} \right] = 0 \quad (13)$$

The thermal stress and thermal strain in the laser mirror under the action of a given temperature distribution can be expressed by the thermoelasticity equation [19].

Equilibrium equations

$$\begin{aligned} \frac{\partial \sigma_r}{\partial r} + \frac{\partial \tau_{rz}}{\partial z} + \frac{\sigma_r - \sigma_\theta}{r} &= 0 \\ \frac{\partial \tau_{rz}}{\partial r} + \frac{\partial \sigma_z}{\partial z} + \frac{\tau_{rz}}{r} &= 0 \end{aligned} \quad (14)$$

Geometry equations

$$\begin{aligned} \varepsilon_r &= \frac{\partial u_r}{\partial r}, \quad \varepsilon_\theta = \frac{u_r}{r}, \quad \varepsilon_z = \frac{\partial u_z}{\partial z} \\ \gamma_{rz} &= \frac{\partial u_r}{\partial z} + \frac{\partial u_z}{\partial r} \end{aligned} \quad (15)$$

Physics equations

$$\begin{aligned} \sigma_r &= \lambda \varepsilon + 2G\varepsilon_r - \frac{E}{1-2\nu} \alpha_T (T - T_0) \\ \sigma_\theta &= \lambda \varepsilon + 2G\varepsilon_\theta - \frac{E}{1-2\nu} \alpha_T (T - T_0) \\ \sigma_z &= \lambda \varepsilon + 2G\varepsilon_z - \frac{E}{1-2\nu} \alpha_T (T - T_0) \\ \tau_{rz} &= G\gamma_{rz}, \quad \varepsilon = \varepsilon_r + \varepsilon_\theta + \varepsilon_z \\ G &= \frac{E}{2(1+\nu)} \end{aligned} \quad (16)$$

where  $\lambda$  is Lamé constant, expressed as  $\lambda = E\nu/(1+\nu)(1-2\nu)$ .

### 3. Numerical simulation

As mentioned in the part of Analysis, the geometry structure of the model used in Comsol Multiphysics is the mirror layer part in Fig. 1. ‘General Heat Transfer’ mode is applied to calculate heat transfer by conduction and convection, while ‘Solid, Stress–Strain’ mode is applied to calculate the thermal stress and strain. For ‘General Heat Transfer’ mode, initial temperature of the model is considered as ambient temperature, which is,

$$T|_{t=0} = T_0 \quad (17)$$

Boundary condition of irradiation region is constant heat flux, which equals the absorbed light intensity, expressed as,

$$-k \frac{\partial T}{\partial z} \Big|_{z=d, 0 \leq r \leq r_0} = (1 - \eta)I(r, t) \quad (18)$$

Boundary condition of cooling region is the convection between cooling water and mirror wall, represented as,

$$-k \frac{\partial T}{\partial z} \Big|_{z=0, 0 \leq r \leq r_1} = h(T - T_c) \quad (19)$$

Boundary conditions of other region are thermal insulation, expressed as,

$$\begin{aligned} -k \frac{\partial T}{\partial z} \Big|_{z=d, r_0 < r \leq r_2} &= 0 \\ -k \frac{\partial T}{\partial z} \Big|_{z=0, r_1 < r \leq r_2} &= 0 \\ -k \frac{\partial T}{\partial z} \Big|_{0 \leq z < d, r=r_2} &= 0 \end{aligned} \quad (20)$$

The heat transfer coefficient ( $h$ ) is calculated according to equations (6)–(9). The corresponding total heat exchanger area can be obtained based on equation (12). However, the heat exchanger area cannot be expressed in the calculation model because the geometry structure of the model is just the mirror layer part. So, an effective heat transfer coefficient ( $h_e$ ) is adopted; and corresponding heat exchanger area is replaced by the area of cooling region. The effective heat transfer coefficient ( $h_e$ ) is expressed as,

$$h_e = h \cdot A / \pi \cdot r_1^2 \quad (21)$$

For ‘Solid, Stress–Strain’ mode, the constraint condition of axial boundary is fixed, while the constraint condition of radial boundary is free.

Some hypothetical conditions for numerical simulation and physical properties of silicon are listed in Tables 1 and 2, respectively. Besides the hypothetical conditions in Table 1, the following assumptions are predefined: laser irradiation is uniform; the thermal deformation is the deformation along  $z$  direction; the flow in microchannels is laminar flow; the natural convective heat transfer is negligible; the physical properties of the mirror and water are constants; the temperature of cooling water and ambient temperature are both 293 K.

Under the hypothetical conditions in Table 1, the temperature rise of the mirror with cooling is less than 5 K. Therefore, it is reasonable to neglect the natural convection. Besides, the Reynolds number in microchannels is less than 1000; and the maximal temperature rise of cooling water is about 0.4 K (supposing the laser energy absorbed totally by cooling water). So, it is reasonable to assume that the flow in microchannels is laminar flow and the temperature of cooling water is constant. Moreover, the mesh size is small enough to validate the simulation results independent of mesh size.

### 4. Results and discussion

The effect of laser power on the temperature rise and thermal deformation on the mirror surface is analyzed under the condition

**Table 1**  
Hypothesis conditions for numerical simulation.

Hypothesis conditions	Value	Unit
Laser power density ( $I(r,t)$ )	200	W/cm <sup>2</sup>
Reflectivity ( $\eta$ )	99	%
Mirror thickness ( $d$ )	2.0	mm
Mirror radius ( $r_2$ )	28.5	mm
Cooling region radius ( $r_1$ )	23.5	mm
Irradiation region radius ( $r_0$ )	15.0	mm
Channel width ( $a$ )	1.0	mm
Channel depth ( $b$ )	2.0	mm
Fin width ( $c$ )	1.5	mm
Water flow rate ( $Q$ )	500	mL/min

**Table 2**  
Physical properties of silicon.

$\rho$ (kg/m <sup>3</sup> )	$k$ (W/m K)	$E$ (GPa)	$\alpha_T$ (10 <sup>-6</sup> K <sup>-1</sup> )	$c_p$ (J/kg K)	$\nu$ (1)
2329	153	190	2.63	713	0.28

of no cooling. Subsequently, the effect of other parameters will be analyzed with cooling. All parameter values are fixed in Table 1 except the target one during the analysis procedure.

**4.1. Analysis of the mirror surface under different laser powers without cooling**

The temperature rise and thermal deformation on the mirror surface are analyzed after the mirror surface being irradiated for the duration of 10 s by different laser powers under the condition of no cooling, while other relevant parameters are fixed as shown in Table 1.

Fig. 3 presents the temperature rise and the thermal deformation distribution on the mirror surface after being irradiated for the duration of 10 s by different laser powers. From Fig. 3, it clearly shows that the temperature rise and the thermal deformation on the mirror surface would increase in respond to the increase of the laser power level. Moreover, the maximal temperature rise exceeds 15 K under the laser power of 150 W/cm<sup>2</sup> and the corresponding maximal thermal deformation reaches around 0.080  $\mu\text{m}$ , which is more than one-tenth of He–Ne laser wavelength (632.8 nm). Therefore, it is necessary to cool down the mirror in order to ensure the beam quality of the laser, by controlling the thermal deformation being less than one tenth of He–Ne laser wavelength.

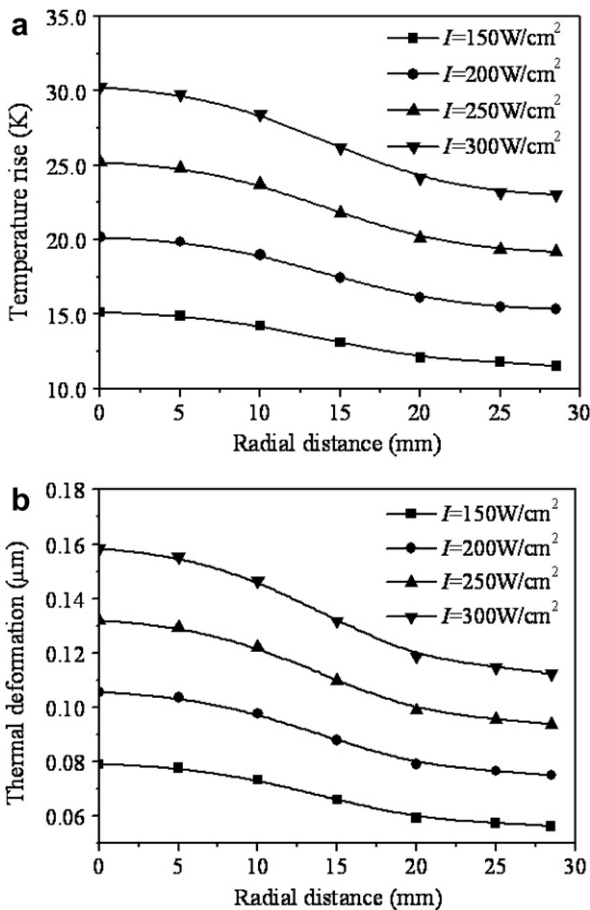


**Fig. 3.** Temperature rise and thermal deformation on the mirror surface under different laser powers.

**4.2. Transient analysis of the mirror surface with cooling**

Under the conditions in Table 1, the temperature rise and the thermal deformation on the mirror surface are analyzed after the mirror surface being irradiated for different time durations with cooling. Fig. 4 shows the temperature rise increases as the time elapses and then inclines to stable state after 10 s both in the mirror centre along axial direction (from the cooling face to the irradiating face) and on the mirror surface along the radial direction at different time, respectively. It is shown that the

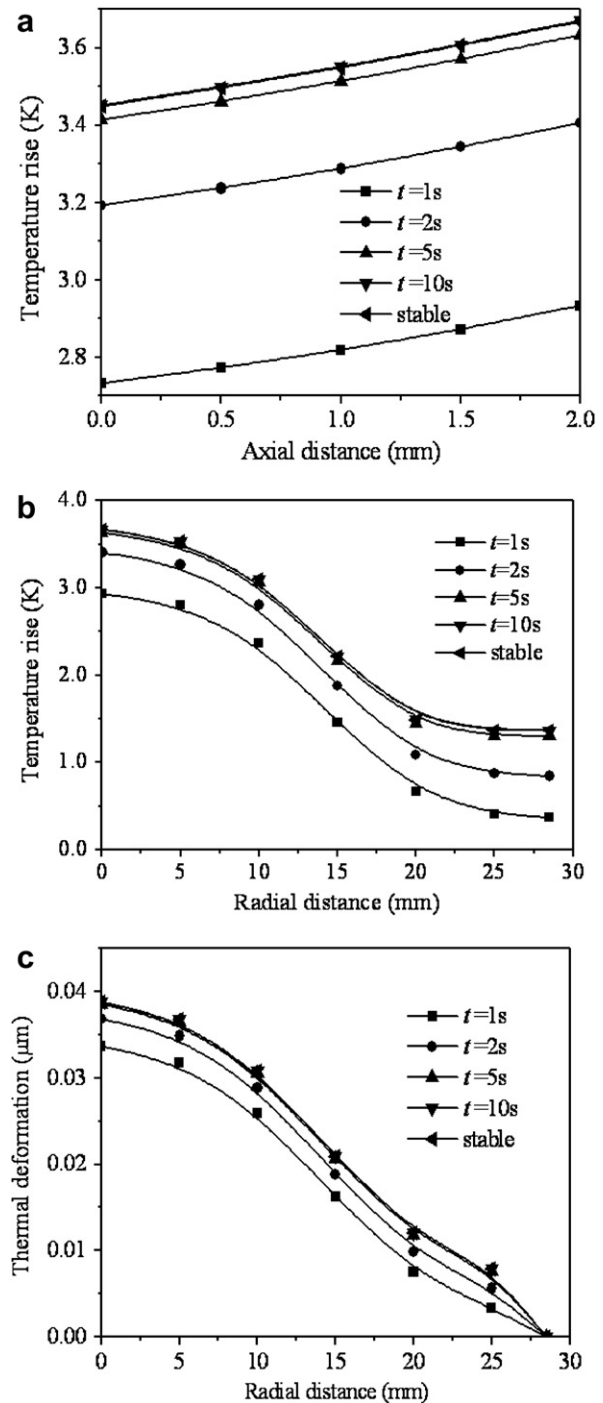


**Fig. 4.** Temperature rise in the mirror centre along axial direction and temperature rise and thermal deformation on the mirror surface along radial direction.

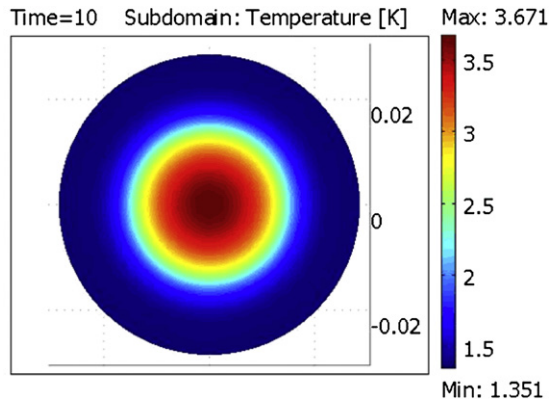


Fig. 5. Temperature rise distribution on the mirror surface at the moment of 10 s.

temperature rise in the mirror centre increases slowly along axial direction at different time and the increasing extent of temperature rise is less than 1 K. Therefore, the thermal deformation on the mirror surface can be evaluated qualitatively from temperature rise on the mirror surface. In other words, the thermal deformation increases with the increasing temperature rise on the mirror surface. Fig. 4 presents that the temperature rise on the mirror surface decreases along the radial direction. The maximal temperature rise has decreased from more than 20 K to lower than 4 K under the laser power of 200 W/cm<sup>2</sup> compared with the

condition of no cooling. As shown in Figs. 3 and 4, the corresponding maximal thermal deformation has reduced from about 0.115 μm to around 0.040 μm (less than one tenth of He–Ne laser wavelength). So, the beam quality of the laser could be ensured effectively. The detailed temperature rise distribution on the mirror surface at the moment of 10 s is shown in Fig. 5.

#### 4.3. Effect of channel width

The effect of channel width on temperature rise and thermal deformation on the mirror surface is analyzed when other conditions are fixed in Table 1. As seen from Fig. 6, the temperature rise increases with increasing the channel width. When channel width changes from 0.5 mm to 2.0 mm ( $b/a \geq 1$  at this stage), the Nusselt number would decrease in respond to the increase of channel width (shown in Fig. 3); and heat transfer coefficient decreases because of the decreasing hydraulic diameter of the channel. Besides, the increase of the channel width has caused the decrease of the channel numbers, which further lead to the decrease of the heat exchange area. When channel width increases to 2.5 mm, the Nusselt number continuously decreases, because the value of depth to width ratio is less than 1 but over 0.6, at which the Nusselt number reaches a low plateau according to Fig. 3. Meanwhile, the corresponding heat transfer coefficient and the heat exchange area decrease as well. Thus, the heat transfer performance of microchannel heat sink decreases with the increased channel width because of the decreasing product of heat transfer coefficient and the heat

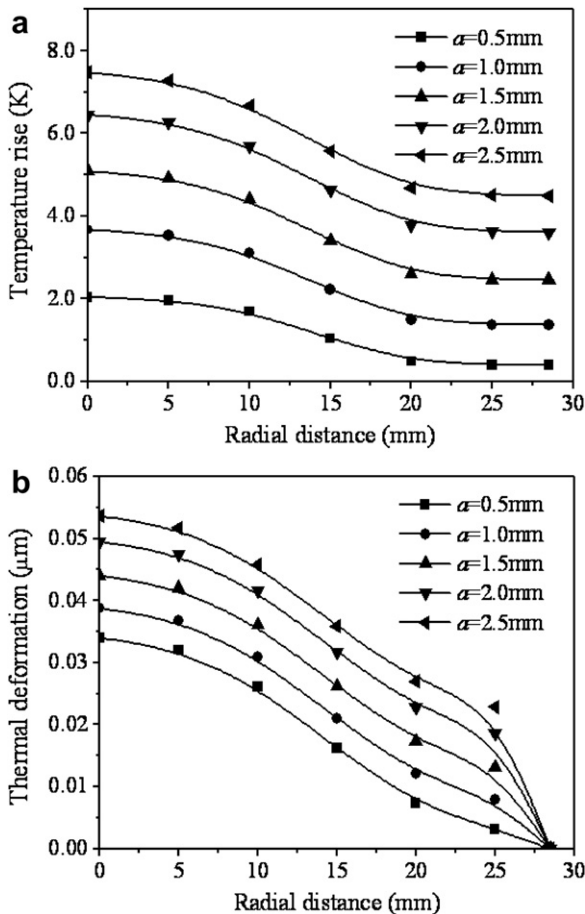


Fig. 6. Effect of channel width on the temperature rise and thermal deformation on the mirror surface.

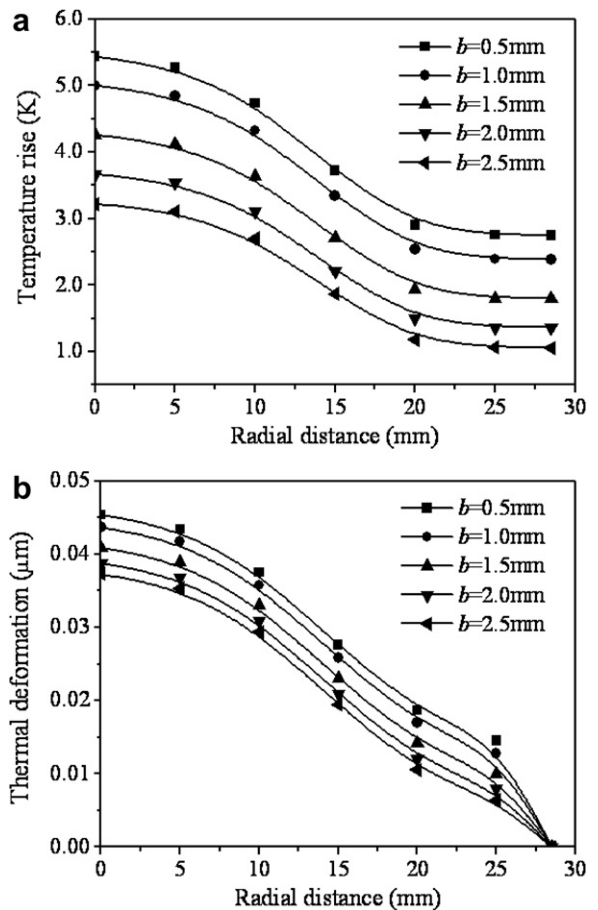


Fig. 7. Effect of channel depth on the temperature rise and thermal deformation on the mirror surface.

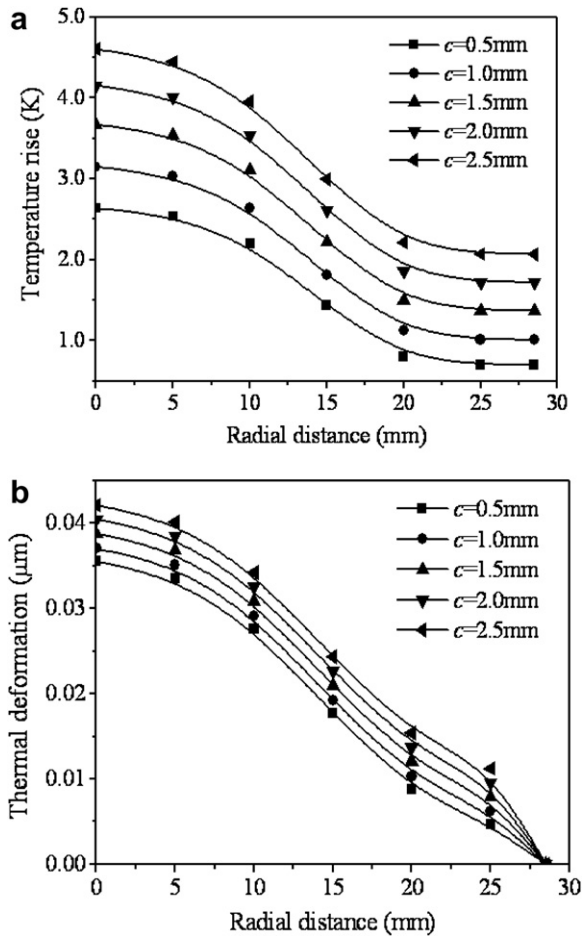


Fig. 8. Effect of fin width on the temperature rise and thermal deformation on the mirror surface.

exchange area. In addition, it could be concluded that the thermal deformation decreases as the temperature rise decreases and the maximal thermal deformation is around  $0.055 \mu\text{m}$ , which is less than one-tenth of He–Ne laser wavelength.

#### 4.4. Effect of channel depth

From Fig. 7 we can see that the temperature rise on the mirror surface decreases in the radial direction with the increase of the channel depth. It is due to the increased product of heat transfer coefficient and the heat exchange area with the increase of the channel depth. Furthermore, the analysis procedure is similar to the one of analyzing the effect of channel width. In Fig. 7, it can be seen that the thermal deformation decreases from about  $0.002 \mu\text{m}$  to  $0.003 \mu\text{m}$  corresponding to every  $0.5 \text{ mm}$  increment of channel depth. The maximal thermal deformation decrease occurs when the channel depth changes from  $1.0 \text{ mm}$  to  $1.5 \text{ mm}$  because of the relatively large increasing amount of the Nusselt number in this case.

#### 4.5. Effect of fin width

As shown in Fig. 8, the temperature rise on the mirror surface would increase if the fin width is increased. The increase of the fin width leads to the decrease of the channel numbers, which further cause the decrease of the heat exchange area. At the same time, heat transfer coefficient keeps invariant because of constant channel width and channel depth. Therefore, the

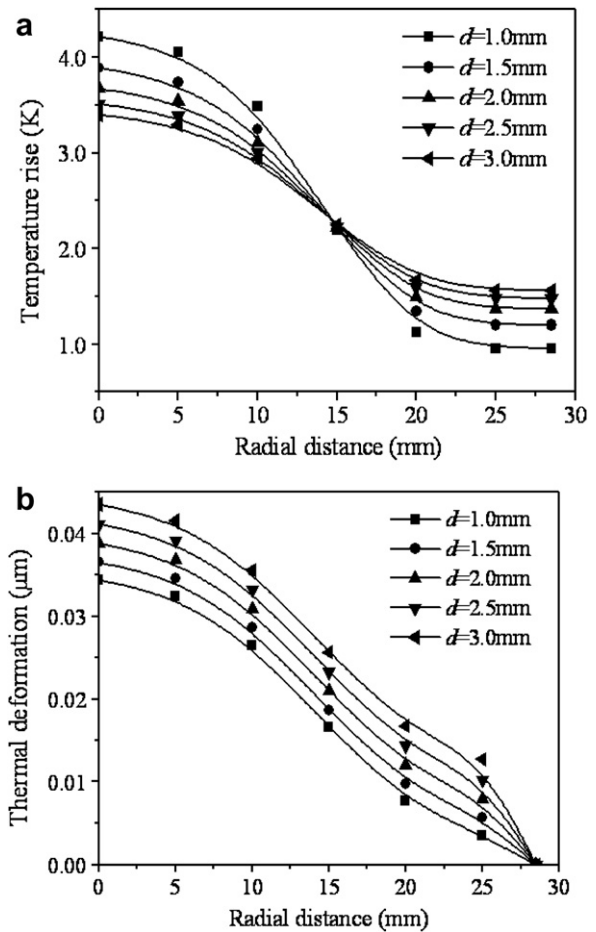


Fig. 9. Effect of mirror thickness on the temperature rise and thermal deformation on the mirror surface.

maximal thermal deformation could be gradually improved with the decreased fin width.

#### 4.6. Effect of mirror thickness

In Fig. 9, it is shown clearly that the temperature rise on irradiation region of the mirror surface decreases with the increase of the mirror thickness. Under the condition of the same laser power and reflectivity, the smaller the mirror heat capacity is, the higher the average mirror temperature is. That is why the maximal temperature rise occurs in the mirror of  $1.0 \text{ mm}$  thickness, and minimal temperature rise occurs in the mirror of  $3.0 \text{ mm}$  thickness. Besides, the conduction through the mirror along the radial direction increases with the increase of mirror thickness, because of the increasing cross sectional area of the mirror. That is why the difference of temperature rises between the irradiation region and the non-irradiation region decreases with the increase of the mirror thickness. Furthermore, it can be found that the thermal deformation decreases as the mirror thickness decreases. This is due to the thermal deformation accumulates along axial direction and is not influenced by the increasing temperature rise gradient along the radial direction. This implies that if the temperature rise gradient is the same, the thinner the mirror thickness is, the less the thermal deformation is. Consequently, under the condition that the rigidity requirement of the mirror is satisfied, it is better to choose the thinner mirror.

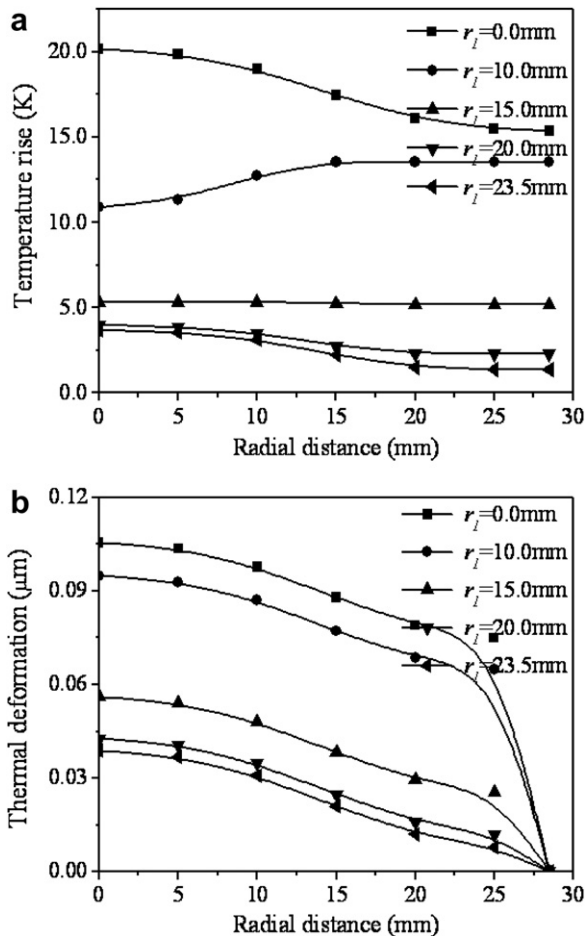


Fig. 10. Effect of cooling region on the temperature rise and thermal deformation on the mirror surface.

#### 4.7. Effect of cooling region

From Fig. 10, it demonstrates that the temperature rise and the thermal deformation on the mirror surface are greatly decreased by using the microchannel heat sink. Under the same effective heat transfer coefficient ( $3950 \text{ W/m}^2 \text{ K}$ ) which is determined by the dimensions of channels in Table 1, the temperature rise on the mirror surface decreases with the increase of cooling region. When the irradiation region radius is larger than the cooling region radius, the temperature rise on the mirror surface is higher on the edge of the mirror and lower in the middle, since the edge of the mirror is not cooled down by the cooling water via convection directly. However, when the irradiation region radius is less than cooling region radius, the temperature rise on the mirror surface distribution is changed in the opposite way. While irradiation region radius equals to the cooling region radius, temperature rise gradient on the mirror surface approaches to zero. Compared with non-irradiation region, the extra heat irradiation region absorbs from laser releases to the cooling water. Moreover, the thermal deformation gradient on the mirror surface is not obviously decreased as the temperature rise gradient on the mirror surface approaches to zero, as the thermal deformation is mainly induced by the temperature rise gradient along the axial direction. Therefore, under the same heat transfer coefficient, the cooling region should be designed as large as possible in order to obtain the minimum thermal deformation.

## 5. Conclusions

The thermal deformation on the mirror surface could be controlled less than one-tenth of He–Ne laser wavelength and the laser beam quality can be ensured by using microchannel heat sink designed. Under hypothetical conditions of numerical simulation, the temperature rise on the mirror surface inclines to stable state after 10 s. For the geometric structure of the microchannel, under the same diameter of the cooling region, the heat exchange area increases in respond to the increase of the channel depth. However, it would decrease if the channel width and the fin width increase. Therefore, high aspect ratio (depth to width ratio) is favorable to improve the heat transfer performance of the microchannel heat sink. Meanwhile, the thermal deformation can be further decreased. Under the condition that the rigidity requirement of the mirror is satisfied, it is better to choose the thinner mirror. With the same heat transfer coefficient, the cooling region should be designed as large as possible in order to obtain the minimal thermal deformation.

## Acknowledgments

We gratefully acknowledge the financial support of the National Natural Science Foundation of China (No. 20490208).

## References

- [1] Y.F. Peng, Z.H. Cheng, Y.N. Zhang, J.L. Qiu, Laser-induced temperature distributions and thermal deformations in sapphire, silicon, and calcium fluoride substrates at  $1.315 \mu\text{m}$ . *Optical Engineering* 40 (12) (2001) 2822–2829.
- [2] M. Kasamatsu, K. Tsukamoto, S. Shiratori, A. Obara, F. Uchiyama, JP Patent No.55–148461, 1982.
- [3] J. Bluege, US Patent No. 5076348, 1991.
- [4] J.H. Rosenfeld, M.T. North, Porous media heat exchangers for cooling of high-power optical components. *Optical Engineering* 34 (2) (1995) 335–341.
- [5] K.H. Lee, O.J. Kim, Analysis on the cooling performance of the thermoelectric micro-cooler. *International Journal of Heat and Mass Transfer* 50 (9–10) (2007) 1982–1992.
- [6] M.L. Ma, J. Guo, L.M. Zhang, F. Yang, Study on the control of micro-deformation of resonator mirrors and windows in high power laser. *Electronics Optics and Control* 14 (1) (2007) 81–84.
- [7] W.L. Zheng, Z.W. Li, B.C. Liu, Q. Tian, The development of research of thermoelectrics. *College Physics* 23 (11) (2004) 55–57.
- [8] D.B. Tuckerman, R.F.W. Pease, High-performance heat sinking for VLSI. *IEEE Electron Device Letters* 2 (5) (1981) 126–129.
- [9] P.Y. Wu, W.A. Little, Measurement of the heat transfer characteristics of gas flow in fine channel heat exchanger used for microminiature refrigerators. *Cryogenics* 24 (8) (1984) 415–420.
- [10] M.M. Rahman, F.L. Gui, Experimental measurements of fluid flow and heat transfer in microchannel cooling passages in a chip substrate, *Proceedings of the ASME International Electronics Packaging Conference*, Binghamton, NY, USA, 1993, pp.685–692.
- [11] B.X. Wang, X.F. Peng, Experimental investigation on liquid forced-convection heat transfer through microchannels. *International Journal of Heat and Mass Transfer* 37 (Suppl. 1) (1994) 73–82.
- [12] T.M. Harms, M.J. Kazmierczak, F.M. Gerner, Developing convective heat transfer in deep rectangular microchannels. *Journal of Heat and Fluid Flow* 20 (2) (1999) 149–157.
- [13] W.L. Qu, I. Mudawar, Experimental and numerical study of pressure drop and heat transfer in a single-phase micro-channel heat sink. *International Journal of Heat and Mass Transfer* 45 (12) (2002) 2549–2565.
- [14] T.Y. Lin, C.Y. Yang, An experimental investigation on forced convection heat transfer performance in micro tubes by the method of liquid crystal thermography. *International Journal of Heat and Mass Transfer* 50 (23–24) (2007) 4736–4742.
- [15] R.K. Shah, A.L. London, *Laminar Flow Forced Convection in Ducts: A Source Book for Compact Heat Exchanger Analytical Data* (Advances in Heat Transfer. Supplement). Academic Press, New York, 1978, pp. 196–209.
- [16] R.J. Phillips, *Forced Convection, Liquid Cooled, Microchannel Heat Sinks*, thesis (M.S.), Massachusetts Institute of Technology, 1987.
- [17] E.R.G. Eckert, R.M. Drake, *Analysis of Heat and Mass Transfer*. Science Press, Beijing, 1983, pp. 79–97.
- [18] F.P. Incropera, D.P. DeWitt, T.L. Bergman, A.S. Lavine, *Fundamentals of Heat and Mass Transfer*, sixth ed. John Wiley & Sons Inc, 2007, 70–77.
- [19] C.J. Cheng, *Elasticity*. Lanzhou University Press, Lanzhou, 1996, pp. 465–471.